Molecular Motion and Ligand Stacking Influence

Thermal Expansion Behavior and Argentophilic

Forces in Silver Coordination Complexes

Gary C. George III, a Daniel K. Unruh, Ryan H. Groeneman, and Kristin M. Hutchinsa\*

<sup>a</sup> Department of Chemistry and Biochemistry, Texas Tech University, Lubbock, TX, 79409

USA. Email: kristin.hutchins@ttu.edu

<sup>b</sup> Department of Biological Sciences, Webster University, St. Louis, MO, 63119, USA.

ABSTRACT: We designed a series of metal-organic solids using ligands with similar molecular

structures that were expected to afford coordination complexes with similar solid-state structures.

The metal component is silver(I) p-toluenesulfonate, and the ligands differ in their ability to

undergo dynamic molecular motion. Although the ligands are similar in molecular structure, the

metal complexes exhibit different solid-state structures due to differences in  $\pi$ -stacking

arrangements and presence or lack of Ag···Ag interactions. The coordination units (ligand-Ag-

ligand) in each complex respond differently to temperature changes, which results in thermal

expansion behaviors ranging from negative to zero to positive within the series. Two unique

complexes were obtained with the azo-containing ligand, and preparation of each complex in

bulk was controlled by synthetic conditions. Two polymorphs were obtained with the olefin-

containing ligand, and both complexes undergo dynamic molecular motion, although the

supramolecular structures differed dramatically. Overall, we show that simple modifications to ligand structure can significantly affect solid-state structure, crystal form, and subsequent thermal expansion behavior.

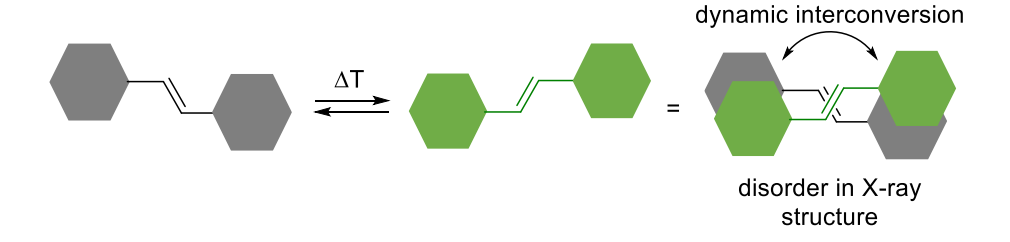
## **INTRODUCTION**

Designing and controlling the response of materials to changes in temperature (i.e., thermal expansion (TE) behavior) within inorganic, metal-organic, and organic solids continues to be an active area of research for materials scientists and crystal engineers. <sup>1-4</sup> The factors that influence TE are generally based upon the molecular structure, chemical bonds, and/or non-covalent interactions that hold the solid material together. <sup>5-7</sup> Small changes in the molecular-level structure can cause significant transformations to the solid-state structure. Moreover, during the synthesis of solid-state materials, different forms or polymorphs can often be obtained by modifying synthetic conditions. Importantly, different material phases frequently give rise to distinct solid-state properties (e.g. solubility, TE, optical), <sup>8-10</sup> so gaining synthetic control over the form obtained is crucial.

Our research groups have an ongoing interest in molecular pedal motion<sup>11</sup> within solid-state materials and the affect that conformational changes have on TE<sup>12, 13</sup> (Scheme 1). Specifically, we have reported the ability to control TE in organic solids containing bipyridine molecules by varying the motion capability of the bridging group between the rings. The TE parameters along the direction where motion occurs in the solid have repeatedly been larger when the molecule undergoes pedal motion as compared to molecules that are unable to undergo motion. Thus far, we have focused primarily on organic solids and symmetric bipyridines containing azo (N=N) or olefin (C=C) bridging groups, which are capable of undergoing pedal

motion, or the acetylene group (C=C) that acts as a control and cannot undergo pedal motion. Recently, we began to investigate metal-organic solids and chose a ligand containing a motion-capable moiety. In our first study, we combined silver(I) trifluoromethane sulfonate with 4-stilbazole, and an order-disorder phase transition of the anion occurred upon heating. We, thus, sought to conduct a more in-depth study using both motion-capable and -incapable ligands that, when combined with a metal, would be expected to form coordination complexes with similar solid-state structures. Our goal was to determine the impact of motion on TE in a series of metal-organic solids without contribution of phase changes, which can affect TE.

**Scheme 1.** Dynamic pedal motion of a stilbene-type molecule.



Here, we report the synthesis, control over crystal form obtained in bulk, and TE behaviors for five discrete coordination complexes containing silver(I) *p*-toluene sulfonate and the unsymmetrical ligands 4-phenylazopyridine (**Azo**), 4-stilbazole (**SB**), or 4-pyridyl acetylene benzene (**PAB**) (Scheme 2a). These ligands differ in their abilities to undergo molecular pedal motion in the solid state; **Azo** and **SB** are motion capable, while **PAB** is not. The silver atoms are expected to interact through argentophilic (Ag···Ag) interactions<sup>15-18</sup> to direct assembly into discrete dimers, which does occur in solids containing **SB** or **PAB** (Scheme 2b). Unexpectedly, we obtained a second polymorph with the **SB** ligand that lacks argentophilic forces entirely. Moreover, when **Azo** is used, two unique crystal forms are obtained. One form, obtained under

faster crystallization conditions, contains two unique supramolecular assemblies within the solidstate structure. One assembly is nearly identical to those observed in the complexes containing SB and PAB. The second assembly contains Azo ligands arranged edge-to-face, which prohibits the silver atoms from engaging in argentophilic interactions. The second crystalline form with Azo is an ethanol solvate obtained under longer crystallization conditions, and the solid contains only edge-to-face stacked ligands and lacks argentophilic interactions. Interestingly, the five complexes exhibit dramatically different TE behaviors along the X<sub>1</sub> direction, ranging from negative to zero to positive TE, due to differences in how the coordination units behave with temperature changes. Along the X<sub>3</sub> direction, the ethanol solvate form of the Azo complex and the two complexes containing the SB ligand underwent the largest TE due to pedal motion (Scheme 1) and changes in argentophilic interaction length with temperature. The complex containing PAB underwent the least TE, due to contribution of the strong Ag-N coordination bonds in the X<sub>3</sub> plane and the lack of a motion-capable group. This study demonstrates that simple modifications to ligand structure can dramatically affect solid-state structure, crystal form, and resulting TE behavior.

**Scheme 2.** Chemical structures of (a) ligands and (b) coordination complexes in this work.

#### **EXPERIMENTAL**

The ligands Azo, SB, and PAB were synthesized using literature or modified literature procedures (see Supporting Information and Figures S8-S10). 19-21 Silver(I) p-toluenesulfonate (Ag p-TolSO<sub>3</sub>) was purchased. Coordination complexes were synthesized by dissolving Ag p-TolSO<sub>3</sub> and the ligand in a 1:2 molar ratio in ethanol (EtOH) for Azo and SB or an EtOH/acetonitrile mixture for PAB. Single crystals suitable for variable-temperature singlecrystal X-ray diffraction (VT SCXRD) studies were grown using slow evaporation over different periods of time. Crystals of the complex containing PAB or SB were obtained over ca. 7 days. Slow evaporation of the solution containing Ag p-TolSO<sub>3</sub> and SB afforded concomitant crystallization of two polymorphs (see SI, section 8). A complex of Ag p-TolSO<sub>3</sub> with PAB has been previously reported by crystallization in ethanol or acetonitrile, and the complex contains a free PAB ligand.<sup>22</sup> We obtained a different form here, and all ligands are coordinated to silver atoms. Two crystal forms were obtained by crystallizing Ag p-TolSO<sub>3</sub> and Azo. Crystals of the non-solvated form of the Azo complex were obtained by shortening the slow evaporation period to 1-2 days, while the EtOH solvated form of the Azo complex was obtained over 5-7 days. SCXRD data for each complex was collected over the temperature range of 290-190 K in 20 K increments (Tables S1-S10). The four coordination complexes were also characterized by <sup>1</sup>H NMR spectroscopy and powder X-ray diffraction (PXRD).

### RESULTS AND DISCUSSION

## Characterization

The coordination complexes  $[Ag(p\text{-TolSO}_3)(\mathbf{SB})_2]$  ( $\alpha$  and  $\beta$  forms),  $[Ag(p\text{-TolSO}_3)(\mathbf{PAB})_2]$ , and  $[Ag(p\text{-TolSO}_3)(\mathbf{Azo})_2]$ EtOH include one unique silver atom, one unique p-

TolSO<sub>3</sub> counterion, and two unique ligands in the asymmetric unit. The EtOH solvate complex also includes one molecule of EtOH in the asymmetric unit. The coordination complex [Ag(p-TolSO<sub>3</sub>)(Azo)<sub>2</sub>] includes two unique silver atoms, two unique p-TolSO<sub>3</sub> counterions, and four unique ligands in the asymmetric unit. Four complexes crystallized in monoclinic space groups; [Ag(p-TolSO<sub>3</sub>)(PAB)<sub>2</sub>] and [Ag(p-TolSO<sub>3</sub>)(Azo)<sub>2</sub>] lie in  $P2_1/n$ , [Ag(p-TolSO<sub>3</sub>)(SB)<sub>2</sub>] ( $\alpha$  form) lies in  $P2_1/c$ , and [Ag(p-TolSO<sub>3</sub>)(Azo)<sub>2</sub>]EtOH lies in C2/c. The fifth complex, [Ag(p-TolSO<sub>3</sub>)(SB)<sub>2</sub>] ( $\beta$  form) lies in the triclinic space group P-1.

The <sup>1</sup>H NMR spectrum of each complex exhibited signals for the p-TolSO<sub>3</sub> counterion and the ligands. The molar ratios of the two components in each NMR spectrum correlated with the ratios observed by SCXRD. The signals corresponding to the ligands within the coordination complexes did not exhibit any significant shifts when compared to the signals of the ligands alone (Figures S11-S14). PXRD demonstrated that the bulk solid material correlated well with the simulated pattern based on SCXRD data (Figures S20-S24). Importantly, the bulk material of each **Azo** complex was controlled through synthetic crystallization time (Figure 1). Fast conditions afforded the non-solvate, while slower conditions afforded the EtOH solvate. The  $\alpha$  and  $\beta$  forms of [Ag(p-TolSO<sub>3</sub>)(**SB**)<sub>2</sub>] crystallized concomitantly (Figure S25-S26).

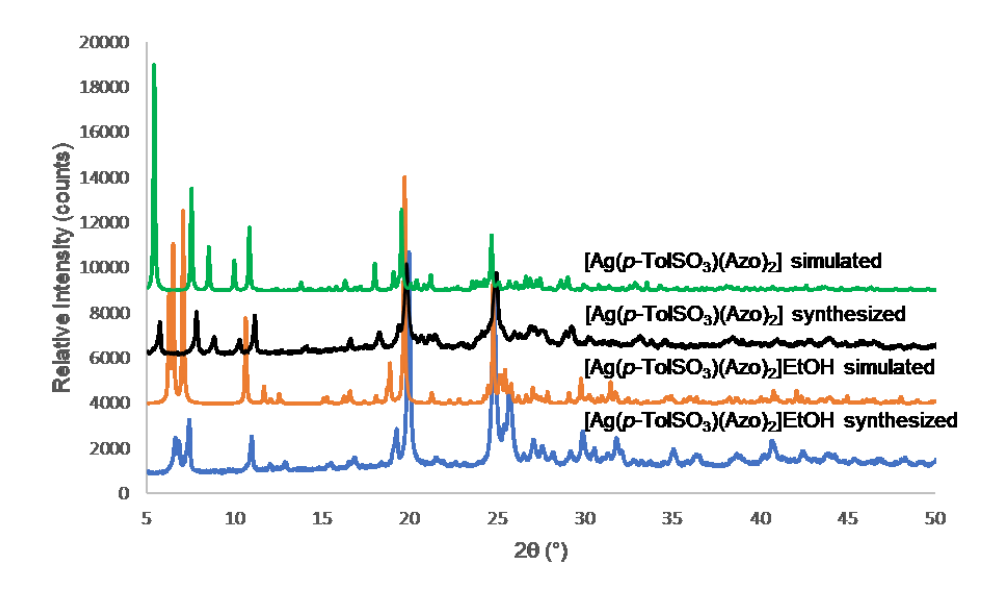


**Figure 1.** Bulk PXRD patterns of synthesized [Ag(p-TolSO<sub>3</sub>)(Azo)<sub>2</sub>] and [Ag(p-TolSO<sub>3</sub>)(Azo)<sub>2</sub>]EtOH and their respective simulated patterns based on SCXRD data.

SCXRD data was collected at six temperatures to analyze the TE behavior and quantify dynamic solid-state pedal motion in the coordination complexes. The components within all five coordination complexes crystallized such that each silver(I) coordinates to two ligands through Ag–N coordination bonds (Table S12). One oxygen atom of the *p*-TolSO<sub>3</sub> counterion coordinates weakly with the silver atom in all coordination complexes at all temperatures (Ag···O distances range from 2.5-2.8 Å). The distance is similar to other reported Ag *p*-TolSO<sub>3</sub> complexes with pyridine ligands.<sup>18, 22-25</sup> The complexes [Ag(*p*-TolSO<sub>3</sub>)(PAB)<sub>2</sub>], [Ag(*p*-TolSO<sub>3</sub>)(Azo)<sub>2</sub>], and [Ag(*p*-TolSO<sub>3</sub>)(Azo)<sub>2</sub>]EtOH exhibit disorder in the sulfonate group. The disorder is present at every temperature for [Ag(*p*-TolSO<sub>3</sub>)(Azo)<sub>2</sub>] (both forms) and at 290 K for [Ag(*p*-TolSO<sub>3</sub>)(PAB)<sub>2</sub>]. Within [Ag(*p*-TolSO<sub>3</sub>)(SB)<sub>2</sub>] (α form), both SB ligands exhibited disorder at every temperature. The disorder was only slightly dynamic as the overall changes were 4% and 9% over the 100 K temperature range studied. For [Ag(*p*-TolSO<sub>3</sub>)(SB)<sub>2</sub>] (β form),

one of the **SB** ligands exhibited disorder at every temperature. The disorder was slightly dynamic as the overall change was also 9% over the 100 K temperature range studied (Table 1).

Within  $[Ag(p-TolSO_3)(Azo)_2]EtOH$ , one **Azo** ligand exhibited disorder at every temperature, and the overall change was 7% over the temperature range (Table 1). There was no crystallographic evidence of disorder in the **Azo** ligands within  $[Ag(p-TolSO_3)(Azo)_2]$  or the **PAB** ligands within  $[Ag(p-TolSO_3)(PAB)_2]$ .

**Table 1.** Major and minor site occupancies for both **SB** ligands in  $[Ag(p-TolSO_3)(SB)_2]$  ( $\alpha$  form), one **SB** ligand in  $[Ag(p-TolSO_3)(SB)_2]$  ( $\beta$  form), and one **Azo** ligand in  $[Ag(p-TolSO_3)(Azo)_2]$ EtOH. The error for each is denoted in parentheses.

Crystal	$[Ag(p-TolSO_3)(SB)_2]$ ( $\alpha$ form)		[Ag(p- TolSO <sub>3</sub> )( <b>SB</b> ) <sub>2</sub> ] (β form)	[Ag(p- TolSO <sub>3</sub> )( <b>Azo</b> ) <sub>2</sub> ]EtOH	
Temperature	Major: minor site occupancies (ligand containing N1, %)	Major: minor site occupancies (ligand containing N2, %)	Major: minor site occupancies (%)	Major : minor site occupancies (%)	
290 K	58(1): 42(1)	59(1):41(1)	88(1):12(1)	89(1):11(1)	
270 K	59(1):41(1)	58(1): 42(1)	90(1):10(1)	90(1): 10(1)	
250 K	60(1):40(1)	57(1):43(1)	92(1):8(1)	92(1):8(1)	
230 K	61(1): 39(1)	55(1):45(1)	94(1):6(1)	94(1):6(1)	
210 K	61(1): 39(1)	52(1):48(1)	96(1):4(1)	95(1):5(1)	
190 K	62(1):38(1)	50(1):50(1)	97(1):3(1)	96(1):4(1)	

## X-ray crystal structure analysis

The coordination units (ligand-Ag-ligand) containing **SB** ( $\alpha$  form) and **PAB** as ligands self-assemble into dimers via argentophilic interactions. For [Ag(p-TolSO<sub>3</sub>)(**SB**)<sub>2</sub>] ( $\alpha$  form) and [Ag(p-TolSO<sub>3</sub>)(**PAB**)<sub>2</sub>], the ligands within the dimer lie face-to-face (Figures 2a and 3a). The Ag···Ag distances within the complexes are 3.31 Å and 3.25 Å for [Ag(p-TolSO<sub>3</sub>)(**SB**)<sub>2</sub>] ( $\alpha$  form) and [Ag(p-TolSO<sub>3</sub>)(**PAB**)<sub>2</sub>], respectively. Both distances are less than the sum of the van der Waals radii for silver atoms (3.44 Å).<sup>26</sup> The extended packing of both complexes is dominated by offset  $\pi$ -stacks of silver dimers (Figures 2b and 3b). Along the c axis, the  $\pi$ -stacks are oriented orthogonally to each other.

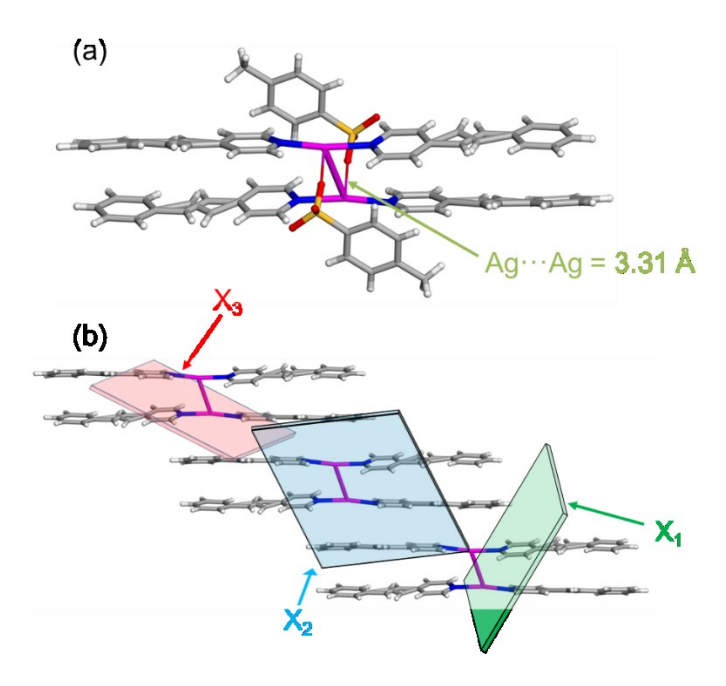


**Figure 2**. X-ray crystal structure of  $[Ag(p-TolSO_3)(SB)_2]$  ( $\alpha$  form) illustrating (a) the silver dimer and (b) packing of neighboring dimers at 290 K. The disorder in the aromatic rings of SB is omitted for clarity, and the p-TolSO<sub>3</sub> counterions are omitted in part b. The directions of the

principal axes of TE are shown by the included planes and arrows, where  $X_1$  is green,  $X_2$  is blue, and  $X_3$  is red.

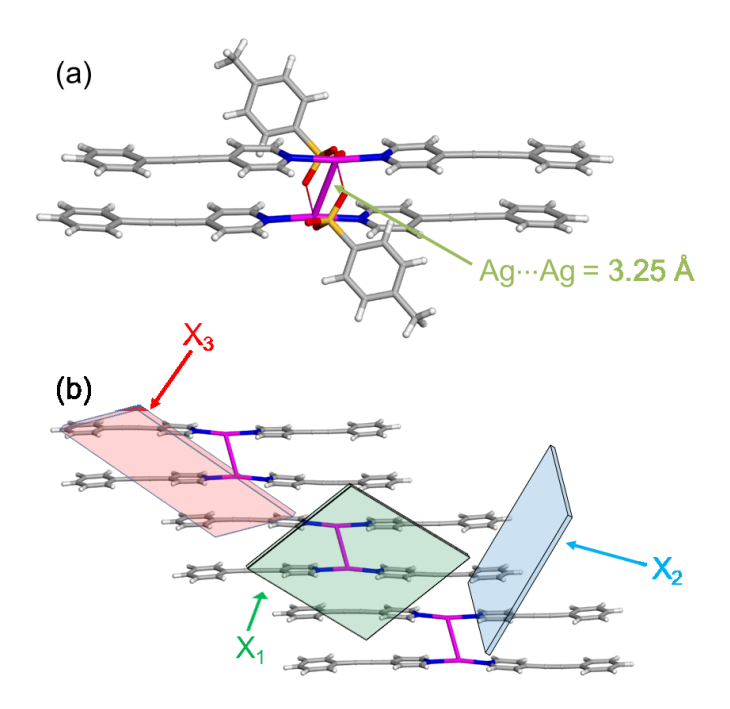


**Figure 3.** X-ray crystal structure of  $[Ag(p-TolSO_3)(PAB)_2]$  illustrating (a) the silver dimer and (b) packing of neighboring dimers at 290 K. The p-TolSO<sub>3</sub> counterions are omitted in part b. The directions of the principal axes of TE are shown by the included planes and arrows, where  $X_1$  is green,  $X_2$  is blue, and  $X_3$  is red.

In the case of [Ag(p-TolSO<sub>3</sub>)(Azo)<sub>2</sub>], which was grown through faster solvent evaporation, there are two unique supramolecular assemblies (Figure 4a). Akin to the two complexes discussed above, one assembly is a dimer, it involves two crystallographically identical silver(I) atoms (Ag1), and the ligands within the dimer lie face-to-face. The Ag···Ag distance between the Ag1 atoms within the dimer is 3.59 Å, which is longer than the analogous distances in the complexes containing SB and PAB and longer than the sum of the van der Waals radii for silver atoms (3.44 Å). The second assembly involves the second unique silver(I) atom

(Ag2), and the ligands within the dimer lie edge-to-face. However, due to the twisting of the ligands into the edge-to-face conformation, the silver(I) atoms are forced farther apart, which prohibits assembly into a true dimer. The Ag···Ag distance between Ag2 atoms is 4.66 Å, which is significantly longer than the sum of the van der Waals radii for silver atoms. The mean planes of the coordination units (Azo-Ag2-Azo) are rotated by  $50^{\circ}$  relative to each other. The face-to-face and edge-to-face assemblies extend along the b axis, and the stacks of face-to-face and edge-to-face assemblies alternate along the crystallographic c axis (Figure 5).

The second crystalline complex containing **Azo**, namely, [Ag(*p*-TolSO<sub>3</sub>)(**Azo**)<sub>2</sub>]EtOH contains only one type of supramolecular assembly. The ligands within the assembly lie edge-to-face and the Ag···Ag distance is 4.58 Å, which also lies outside the sum of the van der Waals radii for silver atoms (Figure 6a). The mean planes of the coordination units (**Azo**-Ag-**Azo**) are rotated by 47° relative to each other. The complex [Ag(*p*-TolSO<sub>3</sub>)(**Azo**)<sub>2</sub>]EtOH also crystallized with highly disordered EtOH in the lattice. The electron density was treated using the Olex2 program's implementation of BYPASS (i.e. SQUEEZE).<sup>27</sup> The void space consisted of 196 electrons per unit cell, which corresponds to 8 ethanol molecules, a volume of 724 Å<sup>3</sup>, and accounts for 12.1% of the total volume (Figure S2).

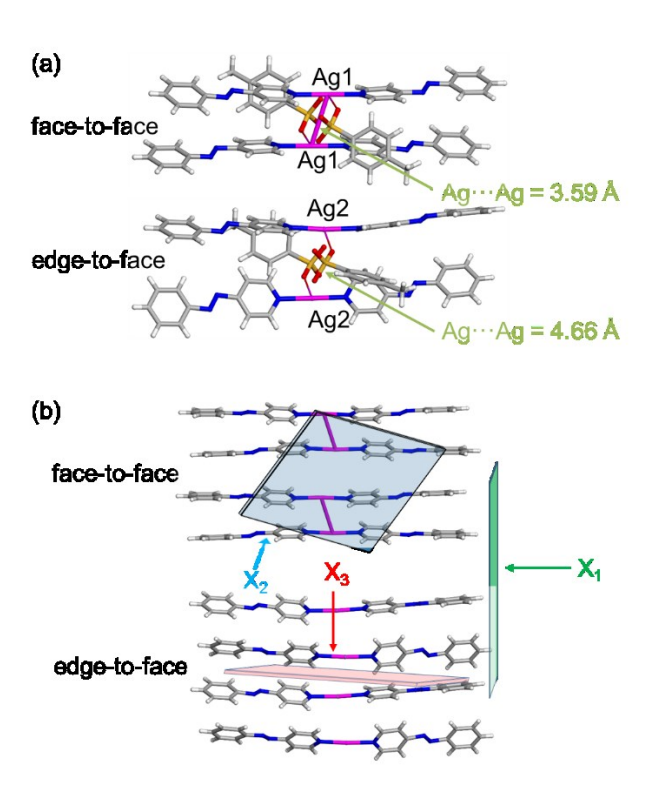


**Figure 4.** X-ray crystal structure of  $[Ag(p-TolSO_3)(Azo)_2]$  at 290 K illustrating (a) the two unique types of assemblies and (b) packing of neighboring assemblies. The p-TolSO<sub>3</sub> counterions are omitted in part b. In part b, the two types of assemblies are not arranged vertically in the crystal structure; they are shown this way to show the TE axes. For packing, see Figure 5 below. The directions of the principal axes of TE are shown by the included planes and arrows, where  $X_1$  is green,  $X_2$  is blue, and  $X_3$  is red.

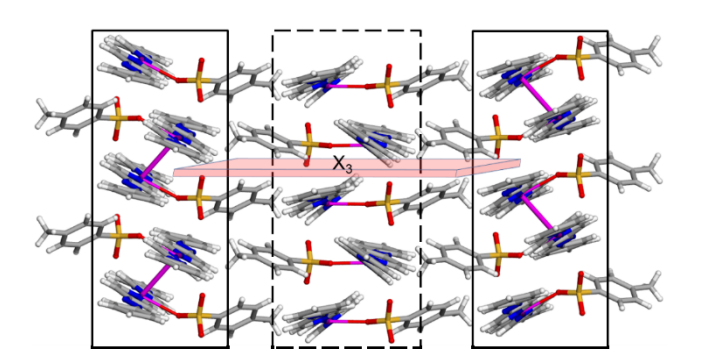


**Figure 5.** Alternating stacks of face-to-face (solid box) and edge-to-face (dashed box) assemblies within  $[Ag(p-TolSO_3)(Azo)_2]$  at 290 K. Principal axis  $X_3$  is shown.

In comparing the two coordination complexes containing Azo, the EtOH solvated form only contains edge-to-face stacked assemblies; thus, the extended structure looks like the edge-to-face portions within the non-solvated form (Figure 7). The non-solvated form was obtained using faster crystallization conditions, while the EtOH solvate form was obtained over slower growth conditions. Given the crystallization conditions and the multiple packing types, the non-solvated form is likely a kinetic product and the solvated form is a more thermodynamically favorable product.

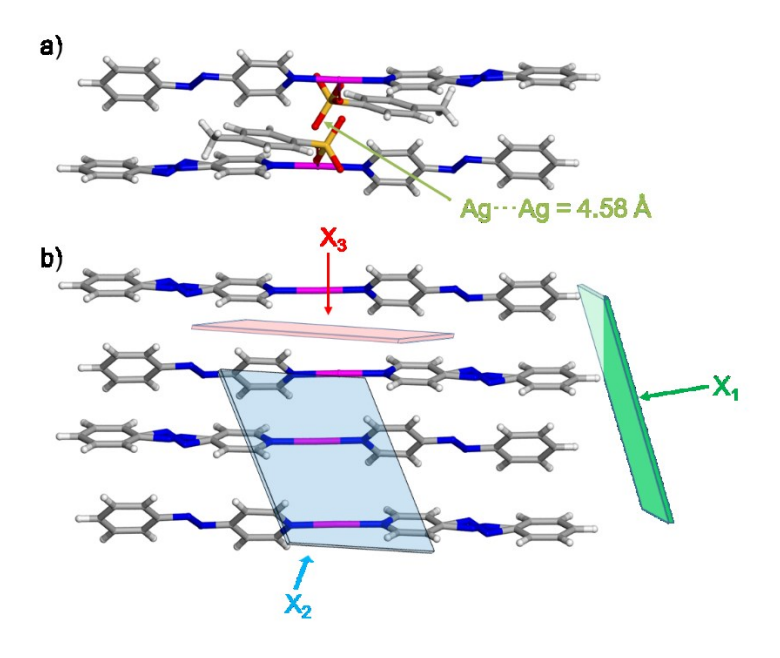


**Figure 6.** X-ray crystal structure of  $[Ag(p-TolSO_3)(Azo)_2]EtOH$  at 290 K illustrating (a) the edge-to-face assembly and (b) packing of neighboring assemblies. The disorder in the aromatic rings of Azo is omitted for clarity, and the  $p-TolSO_3$  counterions are omitted in part b. The

directions of the principal axes of TE are shown by the included planes and arrows, where  $X_1$  is green,  $X_2$  is blue, and  $X_3$  is red.

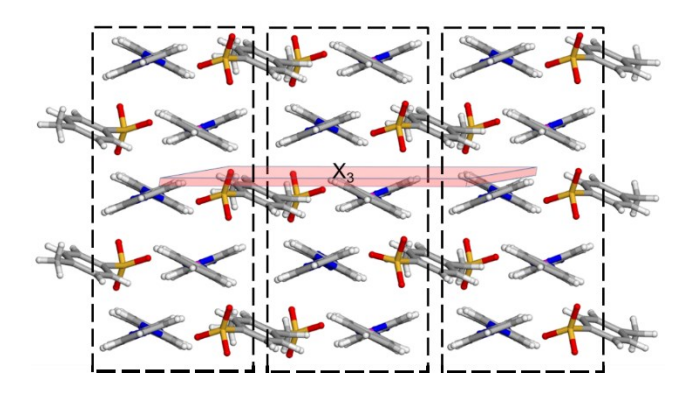


**Figure 7.** Stacks of edge-to-face (dashed box) assemblies within  $[Ag(p-TolSO_3)(Azo)_2]EtOH$  at 290 K. Principal axis  $X_3$  is shown.

As noted above, slow evaporation of the solution containing Ag p-TolSO<sub>3</sub> and **SB** also afforded a polymorph that crystallized concomitantly, namely,  $[Ag(p\text{-TolSO}_3)(\mathbf{SB})_2]$  ( $\beta$  form). The  $\beta$  polymorph contains the components in the same ratio as  $[Ag(p\text{-TolSO}_3)(\mathbf{SB})_2]$  ( $\alpha$  form); however the extended packing differs dramatically from the other four complexes (Figure 8, S27). The silver atoms in the  $\beta$  polymorph are significantly displaced along the c axis, and nearest silver atoms are separated by approximately 6 Å and 12 Å. In this polymorph, half of the **SB** ligands lie face-to-face  $\pi$ -stacked with another ligand; however the ligands are aligned head-to-tail (pyridine rings lie over benzene rings) and coordinated to silver atoms that are nearly 12 Å apart. The other half of the ligands lie edge-to-face with neighboring  $\pi$ -stacked ligands.

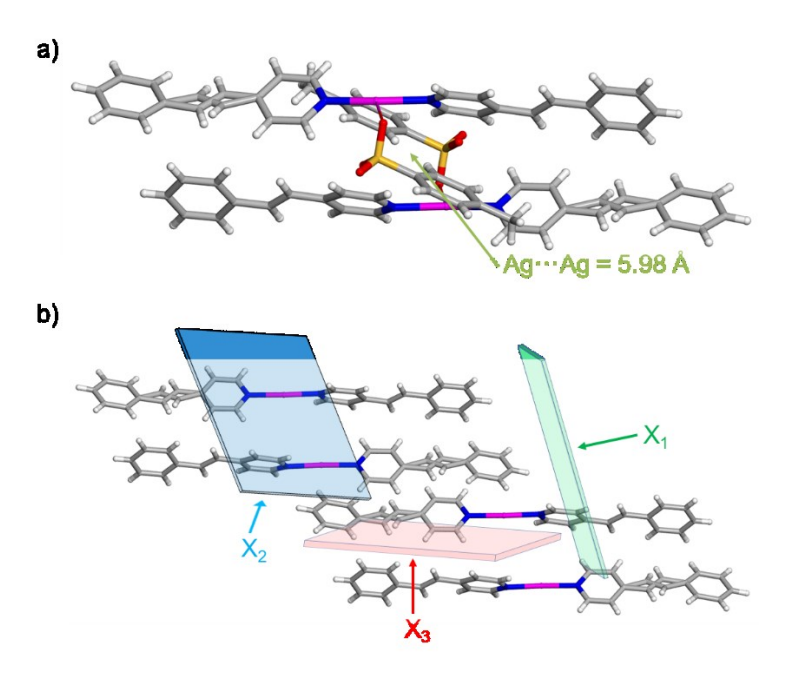


**Figure 8.** X-ray crystal structure of  $[Ag(p-TolSO_3)(SB)_2]$  ( $\beta$  form) at 290 K illustrating (a) the edge-to-face assembly and (b) packing of neighboring assemblies. The disorder in the aromatic rings of SB is omitted for clarity, and the p-TolSO<sub>3</sub> counterions are omitted in part b. The directions of the principal axes of TE are shown by the included planes and arrows, where  $X_1$  is green,  $X_2$  is blue, and  $X_3$  is red.

Argentophilic interactions are a powerful synthon used to direct self-assembly of silver-containing complexes in the solid state.<sup>28-31</sup> Moreover, this assembly often leads to the formation of face-to-face  $\pi$ -stacking between the ligands. Based on this, we were interested in determining how commonly edge-to-face stacking occurs in silver complexes with the three ligands discussed here. A search of the CSD was conducted for structures containing a silver atom and the ligand **Azo**, **SB**, or **PAB**.<sup>32</sup> There were no results for structures containing silver and **Azo**; thus, the two structures reported here are the first. There were eight results for structures containing silver and

**SB**. Of these eight structures, only one structure (CSD Code: GUCZIP)<sup>33</sup> showed a combination of face-to-face and edge-to-face packing in the same structure. There were 12 results for structures containing silver and **PAB**, and none showed a combination of face-to-face and edge-to-face packing in the same structure.

## Thermal expansion behavior

Many metal-organic compounds undergo positive TE in all directions, corresponding to small TE coefficients ( $\alpha = 20 \text{ MK}^{-1}$ ).<sup>34, 35</sup> Currently, the field has termed 'colossal TE' as materials that exhibit TE coefficients equal to or greater than 100 MK<sup>-1,36</sup> PASCal<sup>37</sup> was used to calculate the directions of the three principal axes ( $X_1$ ,  $X_2$ , and  $X_3$ ) and TE coefficients ( $\alpha$ ) for the five coordination complexes using the VT SCXRD data (Table 2, Figures S3-S7 and S15-S19). As noted in Table 2 below, some of the principal axes lie directly along a crystallographic axis and some include a combination of directions. While the five coordination complexes are not isostructural, the TE occurs along comparable crystallographic directions, which allows for comparison across the series. For [Ag(p-TolSO<sub>3</sub>)(SB)<sub>2</sub>] ( $\alpha$  and  $\beta$  forms), [Ag(p-TolSO<sub>3</sub>)(Azo)<sub>2</sub>], and [Ag(p-TolSO<sub>3</sub>)(Azo)<sub>2</sub>]EtOH,  $X_1$  lies along the coordination units,  $X_2$  lies between the neighboring stacks, and  $X_3$  includes the  $\pi$ -stacked direction (Figures 2b, 4b, 6b). For [Ag(p-TolSO<sub>3</sub>)(PAB)<sub>2</sub>], the  $X_1$  and  $X_2$  directions are switched, compared to the other complexes (Figure 3b).

Surprisingly, the five coordination complexes exhibit significantly different TE behavior along the  $X_1$  axis. In  $[Ag(p\text{-TolSO}_3)(\mathbf{Azo})_2]$ , the  $X_1$  axis encompasses the crystallographic a axis.  $[Ag(p\text{-TolSO}_3)(\mathbf{Azo})_2]$  exhibits zero TE because the a axis does not change substantially over the 290-190 K temperature range. The a axis is also the direction of the discrete assemblies (ligand-

Ag-ligand), which do not change substantially in length in response to temperature changes. The complex  $[Ag(p-TolSO_3)(SB)_2]$  ( $\alpha$  form) exhibits negative TE along  $X_1$  due to a decrease in length of the crystallographic b axis upon heating and is also the direction of the discrete assembly, which exhibits slight contraction upon heating. The complex  $[Ag(p-TolSO_3)(SB)_2]$  ( $\beta$ form) also exhibits negative TE along X<sub>1</sub> due to a decrease in length of the crystallographic c axis upon heating and is also the direction of the discrete assembly, which exhibits slight heating. contraction The complexes  $[Ag(p-TolSO_3)(PAB)_2]$ upon and Ag(p-TolSO<sub>3</sub>)(Azo)<sub>2</sub>]EtOH both exhibit positive TE along  $X_1$  due to the a and c crystallographic axes increasing in length upon heating. In  $[Ag(p-TolSO_3)(Azo)_2]$ ,  $[Ag(p-TolSO_3)(SB)_2]$  ( $\alpha$  and  $\beta$ forms) and  $[Ag(p-TolSO_3)(Azo)_2]EtOH$ , the expansion along  $X_1$  occurs in the direction of the strongest interaction, the Ag-N coordination bonds (Figures 2b, 4b, 6b, and 8b, green plane). Interestingly, this same interaction in  $[Ag(p-TolSO_3)(PAB)_2]$  does not lie along the  $X_1$  direction, but instead contributes to the  $X_2$  and  $X_3$  directions. The primary interactions that lie along  $X_1$  for [Ag(p-TolSO<sub>3</sub>)(PAB)<sub>2</sub>] are the Ag···O interactions involving the counterion. All five coordination complexes also include C-H···O and C-H··· $\pi$  interactions in the  $X_1$  direction.

**Table 2**. TE coefficients for the coordination complexes. The errors for the coefficient are in parentheses, and the approximate crystallographic axes are in brackets.

Complex	Ligand stacking	α <sub>X1</sub> (MK <sup>-1</sup> ) [axis]	$\alpha_{X_2}$ (MK <sup>-1</sup> ) [axis]	$\alpha_{X_3}(MK^{-1})$ [axis]	αν(MK <sup>-1</sup> )
$[Ag(p-TolSO_3)(SB)_2]$	face-to-face	-36 (2)	74 (2)	126 (1)	165 (1)
(α form)		[0 -1 0]	[-3 0 -4]	[4 0 1]	
$[Ag(p-TolSO_3)(SB)_2]$	edge-to-face	-18 (1)	23 (1)	170 (1)	175 (1)
(β form)	form)	[-1 -3 4]	[1 3 1]	[-2 1 0]	

	face-to-face	-1 (1)	89 (1)	107 (2)	
$[Ag(p-TolSO_3)(Azo)_2]$	and edge-to- face	[1 0 0]	[0 0 1]	[0 1 0]	196 (2)
[Ag(p-	edge-to-face	19 (1)	52 (1)	145 (5)	217 (7)
TolSO <sub>3</sub> )( <b>Azo</b> ) <sub>2</sub> ]EtOH		[-3 0 -2]	[-1 0 3]	[0 -1 0]	217 (7)
[Ag(p-	face-to-face	42 (2)	69 (1)	72 (1)	196 (5)
$TolSO_3)(\mathbf{PAB})_2]$		[-3 0 5]	[0 1 0]	[-6 0 1]	186 (5)

Four of the five complexes exhibit a similar degree of positive TE along  $X_2$ . The outlier is  $[Ag(p\text{-TolSO}_3)(\mathbf{SB})_2]$  ( $\beta$  form), which exhibits the least TE along  $X_2$ . The  $X_2$  direction for  $[Ag(p\text{-TolSO}_3)(\mathbf{SB})_2]$  ( $\alpha$  and  $\beta$  forms),  $[Ag(p\text{-TolSO}_3)(\mathbf{Azo})_2]$ , and  $[Ag(p\text{-TolSO}_3)(\mathbf{Azo})_2]$ EtOH primarily consists of  $Ag\cdots O$  interactions between stacks of dimers (Figure 3b, 4b, 6b, and 8b, blue planes). All four coordination complexes also include contribution of C-H···O and  $\pi$  interactions to  $X_2$ . Due to the difference in packing,  $[Ag(p\text{-TolSO}_3)(\mathbf{SB})_2]$  ( $\beta$  form) also includes  $Ag\cdots \pi$  interactions, which lie along  $X_2$  and likely contribute to the smaller TE coefficient along  $X_2$ . As outlined above, the  $X_2$  direction for  $[Ag(p\text{-TolSO}_3)(\mathbf{PAB})_2]$  includes the Ag-N coordination bonds and also includes contribution from the  $Ag\cdots Ag$  interactions (Figure 3b, blue plane). Moreover, the coordination unit within  $[Ag(p\text{-TolSO}_3)(\mathbf{PAB})_2]$  exhibits an increase in length upon heating, which contributes to the positive TE.

All five complexes undergo positive TE along  $X_3$  (Figure 2b, 3b, 4b, 6b, and 8b, red planes). The  $\pi$ ··· $\pi$  and Ag···Ag interactions (or separations) are the primary contributor to  $X_3$  in all five coordination complexes. The values for  $[Ag(p\text{-TolSO}_3)(\mathbf{SB})_2]$  ( $\alpha$  and  $\beta$  forms),  $[Ag(p\text{-TolSO}_3)(\mathbf{Azo})_2]$ , and  $[Ag(p\text{-TolSO}_3)(\mathbf{Azo})_2]$ EtOH are colossal, and  $[Ag(p\text{-TolSO}_3)(\mathbf{SB})_2]$  ( $\beta$  form) exhibits the largest coefficient within the series. The  $\pi$ ··· $\pi$  and Ag···Ag interactions

largest changes within  $[Ag(p-TolSO_3)(SB)_2]$  ( $\alpha$  form) and  $[Ag(p-TolSO_3)(SB)_2]$ TolSO<sub>3</sub>)(Azo)<sub>2</sub>]EtOH over the temperature range to facilitate the colossal positive TE (Table S12). Indeed, argentophilic interactions have been shown to facilitate significant expansion in metal-organic materials. 36, 38-40 The complex [Ag(p-TolSO<sub>3</sub>)(SB)<sub>2</sub>] (β form) also includes long  $\pi \cdots \pi$  contacts between the rings of the p-TolSO<sub>3</sub> counterions, which decrease significantly upon cooling to contribute to the larger TE along X<sub>3</sub>. Moreover, the SB ligands within [Ag(p- $TolSO_3)(SB)_2$  ( $\alpha$  and  $\beta$  forms) and Azo ligands within  $[Ag(p-TolSO_3)(Azo)_2]EtOH$  undergo a small amount of dynamic pedal motion over the temperature range, which also contributes to larger TE along  $X_3$ . The TE along  $X_3$  is smaller for  $[Ag(p-TolSO_3)(Azo)_2]$  because the changes in the face-to-face and edge-to-face  $\pi$ ··· $\pi$  stacking distances are smaller and dynamic motion does not occur. Upon cooling [Ag(p-TolSO<sub>3</sub>)(Azo)<sub>2</sub>], the Ag1···Ag1 distance decreases slightly while the Ag2···Ag2 distance increases slightly by a similar length, resulting in less TE. The expansion along  $X_3$  is not colossal for  $[Ag(p-TolSO_3)(PAB)_2]$  due to the contribution of Ag-N coordination bonds to the direction, which are stronger and undergo less change in distance than the  $\pi$ ··· $\pi$ interactions with temperature (Figure S1).

It is interesting to note that the TE along  $X_1$  and  $X_3$  is quite different for the five coordination complexes. Simply by changing the functional group between the coordinating pyridine ring and non-coordinating benzene ring, the TE ranged from negative to zero to positive along  $X_1$ . The ligand structure also affected  $\pi$  stacking and formation of argentophilic forces, which impacted TE along  $X_3$ . The azo group favored edge-to-face stacking and no argentophilic forces, while the acetylene groups favored face-to-face stacking and formation of argentophilic interactions. Interestingly, the two polymorphs containing the olefin ligand exhibited the two extreme assemblies; face-to-face stacking with argentophilic forces ( $\alpha$  form) or edge-to-face

stacking and no argentophilic forces ( $\beta$  form). Small changes to ligand structure also affected molecular motion ability and differences in the behavior of the coordination unit with changing temperature was observed.

#### CONCLUSIONS

Here, we have described the synthesis of five coordination complexes containing silver and unsymmetrical pyridine ligands with functional groups that differ in their ability to undergo molecular pedal motion. The complex containing silver and **PAB** have ligands arranged in face-to-face geometries, aided by argentophilic forces. Two concomitant polymorphs with **SB** were obtained, and one is isostructural to the **PAB** complex, while the second contains no argentophilic forces. Unexpectedly, the complexes containing **Azo** exhibit edge-to-face stacked assemblies and argentophilic forces could not form. Each complex exhibits unique TE behavior along  $X_1$ , due to different behavior in the ligand-Ag-ligand coordination units with change in temperature. All complexes exhibit positive TE along  $X_3$ . The expansion along  $X_3$  is largest for one complex containing **Azo** and both **SB** complexes due to motion and large changes in  $\pi$ -stacking distances with temperature changes. Synthesis of the two **Azo** forms was controlled through crystallization time, and each complex exhibits unique TE behavior. Overall, small changes to ligand structure afforded differences in crystal structure, molecular motion, and response of the solid material to changes in temperature.

#### ASSOCIATED CONTENT

**Supporting Information**. Experimental details, single-crystal X-ray data, powder X-ray diffraction data, thermal expansion data and analysis, NMR spectra, Mercury images, and variation of unit cell parameters with temperature.

**Accession Codes**. CCDC 2156221–2156245 and 2174786–2174791 contain the supplementary crystallographic data for this paper. These data can be obtained free of charge via www.ccdc.cam.ac.uk/structures.

#### **AUTHOR INFORMATION**

# **Corresponding Author**

\*Email: kristin.hutchins@ttu.edu

#### **Notes**

The authors declare no competing financial interest.

#### **ACKNOWLEDGMENT**

KMH gratefully acknowledges financial support from the National Science Foundation DMR-2045506.

#### REFERENCES

- 1. Rather, S. A.; Saraswatula, V. G.; Sharada, D.; Saha, B. K., Influence of molecular width on the thermal expansion in solids. *New J. Chem.* **2019**, *43*, 17146-17150.
- 2. Saraswatula, V. G.; Saha, B. K., A thermal expansion investigation of the melting point anomaly in trihalomesitylenes. *Chem. Commun.* **2015**, *51*, 9829-9832.
- 3. Balestra, S. R. G.; Bueno-Perez, R.; Hamad, S.; Dubbeldam, D.; Ruiz-Salvador, A. R.; Calero, S., Controlling Thermal Expansion: A Metal-Organic Frameworks Route. *Chem. Mater.* **2016**, *28*, 8296-8304.
- 4. Shrivastava, A.; Das, D., Axial Positive, Negative, and Zero Thermal Expansion in a Mixed-Metal Mixed-Linker Coordination Compound: Role of 2D Layer in the Thermal Expansion Property. *Cryst. Growth Des.* **2019**, *19*, 4908-4913.
- 5. Kitaigorodsky, A. I., *Molecular Crystals and Molecules*. Academic Press: 1973.
- 6. Zhang, Z.; Wojtas, L.; Zaworotko, M. J., Three Porphyrin-Encapsulating Metal-Organic Materials with Ordered Metalloporphyrin Moieties. *Cryst. Growth Des.* **2014**, *14*, 1526-1530.
- 7. Zhang, Z.; Zaworotko, M. J., Template-directed synthesis of metal-organic materials. *Chem. Soc. Rev.* **2014**, *43*, 5444-5455.
- 8. Ding, X.; Crawford, A. W.; Derrick, W. P.; Unruh, D. K.; Groeneman, R. H.; Hutchins, K. M., Thermal Expansion Properties and Mechanochemical Synthesis of

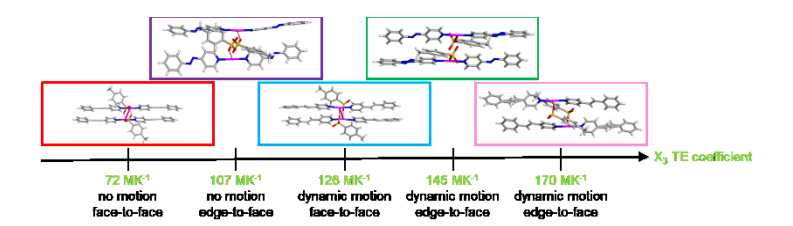
- Stoichiometric Cocrystals Containing Tetrabromobenzene as a Hydrogen- and Halogen-Bond Donor. *Chem. Eur. J.* **2021**, *27*, 16329-16333.
- 9. Fan, Y.; Song, W.; Yu, D.; Ye, K.; Zhang, J.; Wang, Y., Polymorphs and luminescent properties of a cetyl substituted quinacridone derivative. *CrystEngComm* **2009**, *11*, 1716-1722.
- 10. Zhu, B.; Fang, X.; Zhang, Q.; Mei, X.; Ren, G., Study of Crystal Structures, Properties, and Form Transformations among a Polymorph, Hydrates, and Solvates of Apatinib. *Cryst. Growth Des.* **2019**, *19*, 3060-3069.
- 11. Harada, J.; Ogawa, K., Pedal motion in crystals. *Chem. Soc. Rev.* **2009**, *38*, 2244-2252.
- 12. Ding, X.; Unruh, D. K.; Groeneman, R. H.; Hutchins, K. M., Controlling thermal expansion within mixed cocrystals by tuning molecular motion capability. *Chem. Sci.* **2020**, *11*, 7701-7707.
- 13. Hutchins, K. M.; Unruh, D. K.; Verdu, F. A.; Groeneman, R. H., Molecular Pedal Motion Influences Thermal Expansion Properties within Isostructural Hydrogen-Bonded Co-crystals. *Cryst. Growth Des.* **2018**, *18*, 566-570.
- 14. Juneja, N.; Unruh, D. K.; Groeneman, R. H.; Hutchins, K. M., Positive thermal expansion facilitates the formation of argentophilic forces following an order–disorder phase transition. *New J. Chem.* **2021**, *45*, 8898-8901.
- 15. Schmidbaur, H.; Schier, A., Argentophilic Interactions. *Angew. Chemie, Int. Ed.* **2015**, *54*, 746-784.
- 16. van Terwingen, S.; Englert, U., Argentophilic Interactions in Two AgI Complexes of 3-(2-(Pyridin-4-yl)ethyl)pentane-2,4-dione, a Promising Ditopic Ligand. *Crystals* **2019**, *9*, 414.
- 17. Konavarapu, K. S. N.; Biradha, K., Coordination Polymers of M2L2 Macrocycles and M3L2 Podands Containing Tris (pyridyl) Tripodal Amide: Anion Bridging, Ag···Ag Interactions and Solid-State Luminescence. *ChemistrySelect* **2016**, *1*, 2299-2306.
- 18. Laird, R. C.; Sinnwell, M. A.; Nguyen, N. P.; Swenson, D. C.; Mariappan, S. V. S.; MacGillivray, L. R., Intramolecular [2 + 2] Photodimerization Achieved in the Solid State via Coordination-Driven Self-Assembly. *Org. Lett.* **2015**, *17*, 3233-3235.
- 19. Bannwarth, A.; Schmidt, S. O.; Peters, G.; Sönnichsen, F. D.; Thimm, W.; Herges, R.; Tuczek, F., FeIII Spin-Crossover Complexes with Photoisomerizable Ligands: Experimental and Theoretical Studies on the Ligand-Driven Light-Induced Spin Change Effect. *Eur. J. Inorgan. Chem.* **2012**, *2012*, 2776-2783.
- 20. Hutchins, K. M.; Rupasinghe, T. P.; Ditzler, L. R.; Swenson, D. C.; Sander, J. R. G.; Baltrusaitis, J.; Tivanski, A. V.; MacGillivray, L. R., Nanocrystals of a metal-organic complex exhibit remarkably high conductivity that increases in a single-crystal-to-single-crystal transformation. *J. Am. Chem. Soc.* **2014**, *136*, 6778-6781.
- 21. Yu, X.; Guttenberger, N.; Fuchs, E.; Peters, M.; Weber, H.; Breinbauer, R., Diversity-Oriented Synthesis of a Library of Star-Shaped 2H-Imidazolines. *ACS Comb. Sci.* **2015**, *17*, 682-690.
- 22. Knichal, J. V.; Gee, W. J.; Cameron, C. A.; Skelton, J. M.; Gagnon, K. J.; Teat, S. J.; Wilson, C. C.; Raithby, P. R.; Burrows, A. D., Exploring Structure—Property Relationships of Silver 4-(Phenylethynyl)pyridine Complexes. *Eur. J. Inorg. Chem.* **2017**, *2017*, 1855-1867.
- 23. Elacqua, E.; Sinnwell, M. A.; Loren, B. P.; Jurgens, P. T.; Groeneman, R. H.; Reinheimer, E. W.; MacGillivray, L. R., Metal-Organic Coordination versus Hydrogen

- Bonding: Highly Efficient Templated Photocycloadditions of Trisubstituted Isomeric Olefins in the Solid State. *ChemPlusChem* **2016**, *81*, 893-898.
- 24. Bedin, M.; Karim, A.; Reitti, M.; Carlsson, A.-C. C.; Topić, F.; Cetina, M.; Pan, F.; Havel, V.; Al-Ameri, F.; Sindelar, V.; Rissanen, K.; Gräfenstein, J.; Erdélyi, M., Counterion influence on the N–I–N halogen bond. *Chem. Sci.* **2015**, *6*, 3746-3756.
- 25. Carlucci, L.; Ciani, G.; Proserpio, D. M.; Porta, F., Four new 2D porous polymeric frames from the self-assembly of silver triflate and silver tosylate with free-base and Znmetallated 5,10,15,20-tetra(4-pyridyl)porphyrin. *CrystEngComm* **2005**, 7, 78-86.
- 26. Bondi, A., van der Waals Volumes and Radii. *J. Phys. Chem.* **1964**, *68*, 441-451.
- 27. van der Sluis, P.; Spek, A. L., BYPASS: an effective method for the refinement of crystal structures containing disordered solvent regions. *Acta Crystallogr. A.* **1990**, *46*, 194-201.
- Garai, M.; Maji, K.; Chernyshev, V. V.; Biradha, K., Interplay of Pyridine Substitution and Ag(I)···Ag(I) and Ag(I)···π Interactions in Templating Photochemical Solid State [2 + 2] Reactions of Unsymmetrical Olefins Containing Amides: Single-Crystal-to-Single-Crystal Transformations of Coordination Polymers. Cryst. Growth Des. 2016, 16, 550-554.
- 29. Sinnwell, M. A.; Baltrusaitis, J.; MacGillivray, L. R., Combination of Argentophilic and Perfluorophenyl-Perfluorophenyl Interactions Supports a Head-to-Head [2 + 2] Photodimerization in the Solid State. *Cryst. Growth Des.* **2015**, *15*, 538-541.
- 30. Goodwin, A. L.; Keen, D. A.; Tucker, M. G., Large negative linear compressibility of Ag3[Co(CN)6]. *PNAS* **2008**, *105*, 18708-18713.
- 31. Ang, Z. Z.; Laxmi, S.; León, F.; Kooij, J. E. M.; García, F.; England, J., Mechanochemical Synthesis of Tripodal Tris[4-(1,2,3-triazol-5-ylidene)methyl]amine Mesoionic Carbene Ligands and Their Complexation with Silver(I). *Inorg. Chem.* **2021**, 60, 3556-3564.
- 32. CSD Version 5.43 (November 2021 + 1 update).
- 33. Medishetty, R.; Sahoo, S. C.; Mulijanto, C. E.; Naumov, P.; Vittal, J. J., Photosalient Behavior of Photoreactive Crystals. *Chem. Mater.* **2015**, *27*, 1821-1829.
- 34. Evans, J. S. O., Negative thermal expansion materials † J. Chem. Soc., Dalton Trans. 1999, (19), 3317-3326.
- 35. Roy, R.; Agrawal, D. K.; McKinstry, H. A., Very Low Thermal Expansion Coefficient Materials. *Annu. Rev. Mater. Sci.* **1989**, *19*, 59-81.
- 36. Conterio, M. J.; Goodwin, A. L.; Tucker, M. G.; Keen, D. A.; Dove, M. T.; Peters, L.; Evans, J. S. O., Local structure in Ag3[Co(CN)6]: colossal thermal expansion, rigid unit modes and argentophilic interactions. *J. Phys.: Condens. Matter* **2008**, *20*, 255225.
- 37. Cliffe, M. J.; Goodwin, A. L., PASCal: a principal axis strain calculator for thermal expansion and compressibility determination. *J. Appl. Crystallogr.* **2012**, *45*, 1321-1329.
- 38. Liu, Z.; Yang, J.; Yang, L.; Li, X.; Ma, R.; Wang, R.; Xing, X.; Sun, D., Argentophilicity induced anomalous thermal expansion behavior in a 2D silver squarate. *Inorg. Chem. Front.* **2021**, *8*, 1567-1573.
- 39. Guo, L.; Tong, J.; Liang, X.; Köhler, J.; Nuss, J.; Li, Y.; Zheng, L., Silver(i) pyrophosphonates: structural, photoluminescent and thermal expansion studies. *Dalton Trans.* **2011**, *40*, 6392-6400.
- 40. Goodwin, A. L.; Keen, D. A.; Tucker, M. G.; Dove, M. T.; Peters, L.; Evans, J. S. O., Argentophilicity-Dependent Colossal Thermal Expansion in Extended Prussian Blue Analogues. *J. Am. Chem. Soc.* **2008**, *130*, 9660-9661.

# For Table of Contents Only

Molecular Motion and Ligand Stacking Influence Thermal Expansion Behavior and Argentophilic Forces in Silver Coordination Complexes

Gary C. George III, Daniel K. Unruh, Ryan H. Groeneman, and Kristin M. Hutchins



Synopsis: The thermal expansion behaviors of five different silver coordination complexes containing unsymmetrical ligands ranges from moderate to colossal positive. The thermal expansion coefficients vary as a function of ligand packing, presence of argentophilic forces, and dynamic molecular motion within each solid. Overall, simple modifications to ligand structure significantly affect solid-state structure, crystal form, and subsequent thermal expansion behavior.